Electronic supplementary information

Diverse sensor responses from two functionalized tris(phthalocyaninato) Europium ambipolar semiconductors towards three oxidative and reductive gases

Shanshan Liu,[a] Haoyuan Wang,[a] Xiangyang Wang,[a] Shaoren Li,[a] Heyuan Liu,[a]

Yanli Chen,*[a] Xiyou Li*[a]

[a] *College of Science,China University of Petroleum (East China), Qingdao 266580, China.*

Corresponding Author

**E-mail: yanlichen@upc.edu.cn (Y. Chen) and xiyouli@upc.edu.cn (X. Li)*

Caption of Content

Fig.S1. Experimental isotopic pattern for the molecular ion of compounds **1-2** shown in the MALDI-TOF mass spectrum.

Fig.S2. ^{1}H NMR spectrum of compounds **1-2** in $CDCl_3$.

Fig.S3. The molecular dimension of compounds **1-2** obtained using PCMODEL for windows Version 6.0, Serena Software.

Fig.S4. Polarized UV-vis spectra of the LS films of **1-2.**

Fig.S5. XRD pattern recorded in in-plane (grazing incidence) mode for the LS films of **1**(A)-**2**(B).

Fig.S6. Output characteristics (I_{ds} vs. V_{ds}) of ambipolar OFET device based on LS films of **1** (A-B) and **2** (C-D).

Fig.S7. The recovery time for **1-2** films exposed to NO_2 at varied concentration in the range of 0.1-0.85 ppm (exposure: 2 min).

Fig.S8. The time-dependent current evolution curves of the three toxic gases (H_2S, NH_3, and NO_2) in a sequential testing for LS films of **1**(A) and (B).

Fig.S9. The response of the devices for compound **1**(A)-**2**(B) under 0.45 ppm NO_2 exposure of 2 min and 10 min.

Table S1. The orientation angle of the phthalocyanine ring determined from polarized UV-vis absorbance of the LS films of compounds **1-2**.

Table S2. The gate-induced sheet carrier densities (*n*) of the LS films of compounds **1-2**.

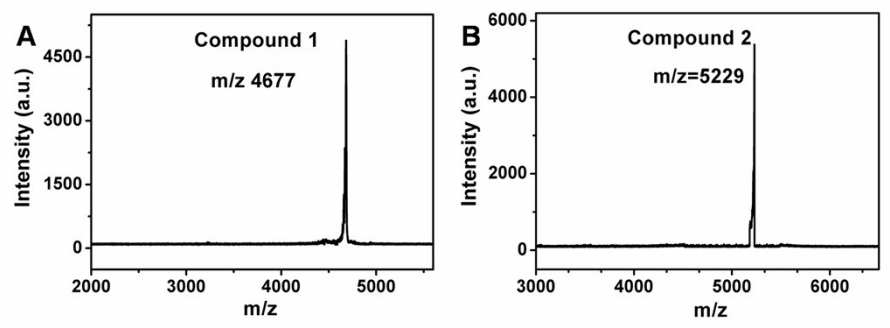

Fig.S1. Experimental isotopic pattern for the molecular ion of $Eu_2[Pc(OC_8H_{17})_8]_2[Pc(OCH_2CF_3)_8]$ (A) and $Eu_2\{Pc[(OC_2H_4)_3OCH_3]_8\}_2[Pc(OCH_2CF_3)_8]$ (B) shown in the MALDI-TOF mass spectrum.

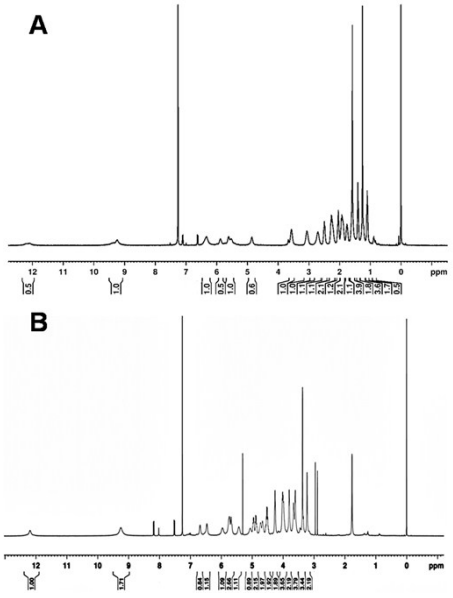

Fig.S2. ^1H NMR spectrum of $Eu_2[Pc(OC_8H_{17})_8]_2[Pc(OCH_2CF_3)_8]$ (A) and $Eu_2\{Pc[(OC_2H_4)_3OCH_3]_8\}_2[Pc(OCH_2CF_3)_8]$ (B) in $CDCl_3$.

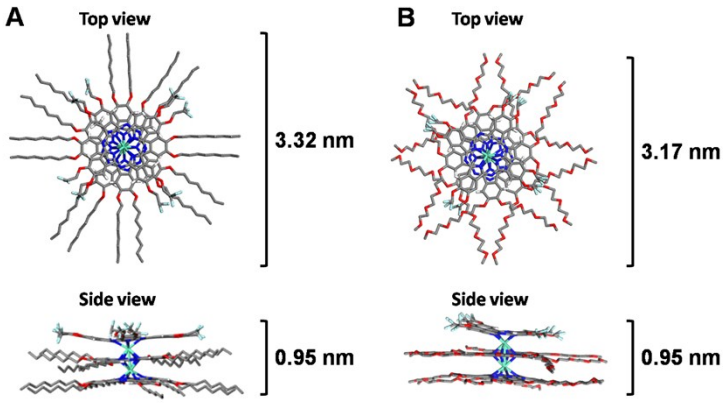

Fig.S3. The molecular dimension of $Eu_2[Pc(OC_8H_{17})_8]_2[Pc(OCH_2CF_3)_8]$(A): 3.32 nm (length) × 0.95 nm (height), $Eu_2\{Pc[(OC_2H_4)_3OCH_3]_8\}_2[Pc(OCH_2CF_3)_8]$(B) : 3.17 nm(length) × 0.95 nm (height) obtained using PCMODEL for windows Version 6.0, Serena Software.

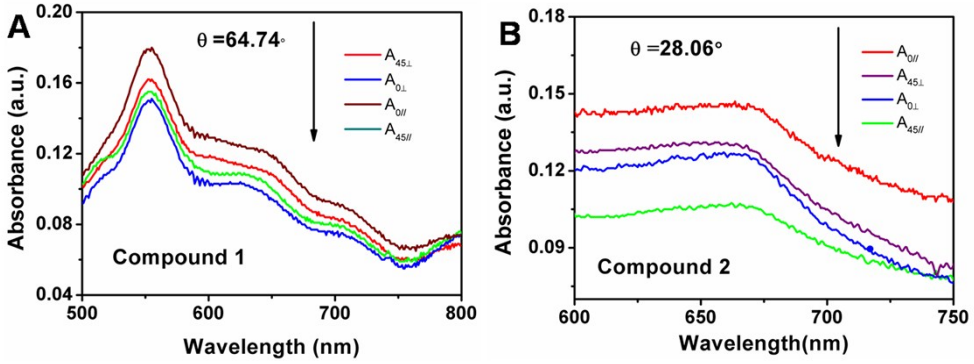

Fig.S4. Polarized UV-vis spectra of compounds **1-2** (A-B) LS films. 0 and 45° represent the angle between the light and the normal of the substrate, respectively, while "A∥ and A⊥" represent the absorbance for light polarized with the electric vector parallel and perpendicular to the dipping direction.

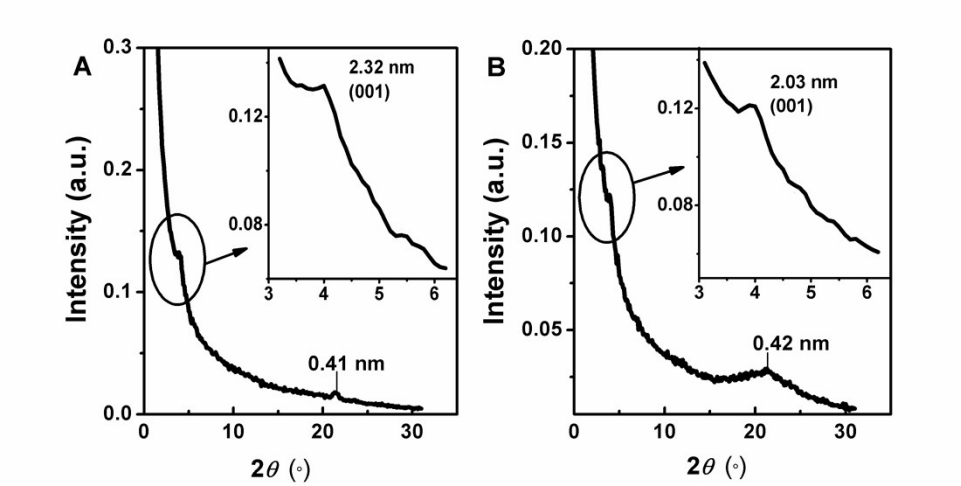

Fig.S5. XRD pattern recorded in in-plane (grazing incidence) mode for the LS films of **1**(A)-**2**(B)**.**

.

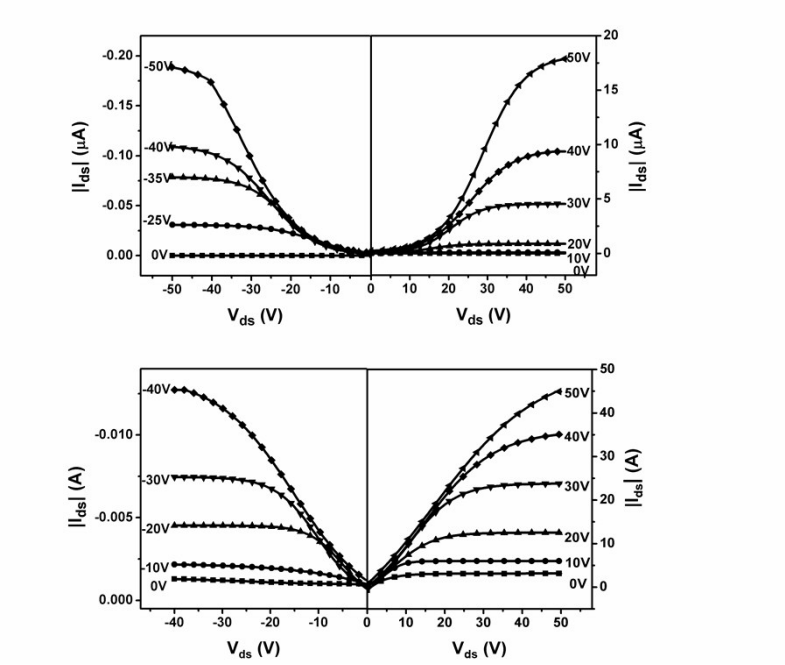

Fig.S6. Current–voltage output plots (I_{ds} vs. V_{ds}) of ambipolar OFET device based on LS films of **1** (A) and **2** (B) deposited on HMDS-treated SiO_2/Si (300 nm) substrate with Au top contacts with various V_G for *p*-channel (left column of A and B) measured in air and for *n*-channel (right column of A and B) measured in N_2, respectively.

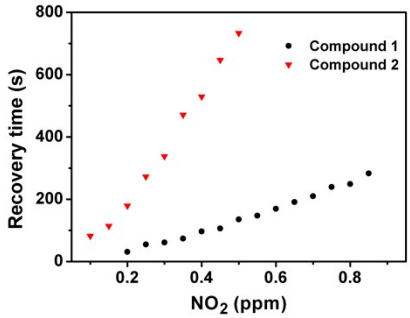

Fig.S7. The recovery time for **1-2** films exposed to NO_2 at varied concentration in the range of 0.1-0.85 ppm (exposure:2 min)

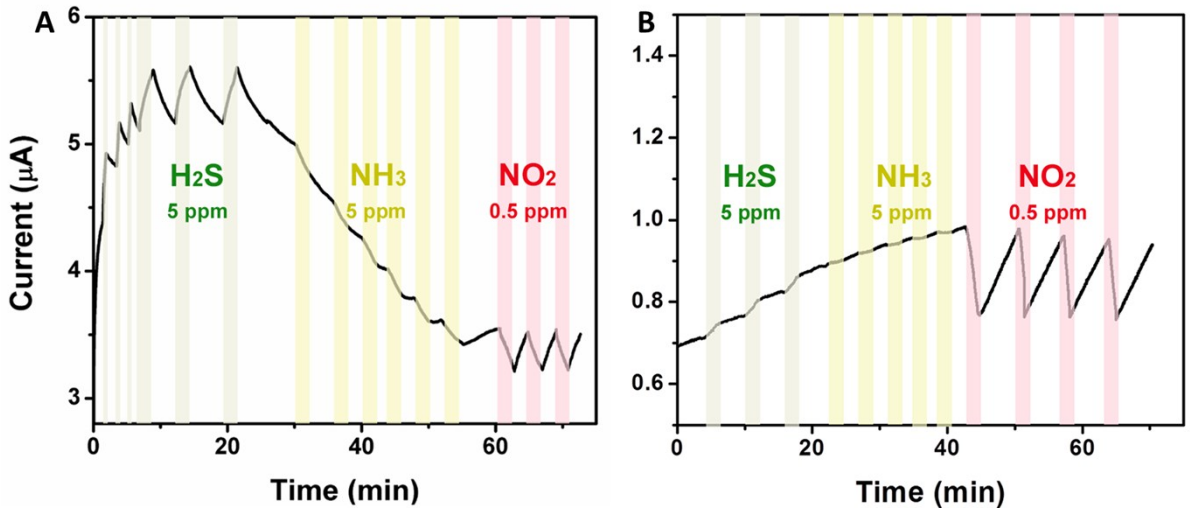

Fig.S8. The time-dependent current evolution curves of the three toxic gases (H_2S of 5 ppm, NH_3 of 5 ppm, and NO_2 of 0.5 ppm) in a sequential testing for LS films of **1**(A) and **2**(B), the color columns represent exposure time.

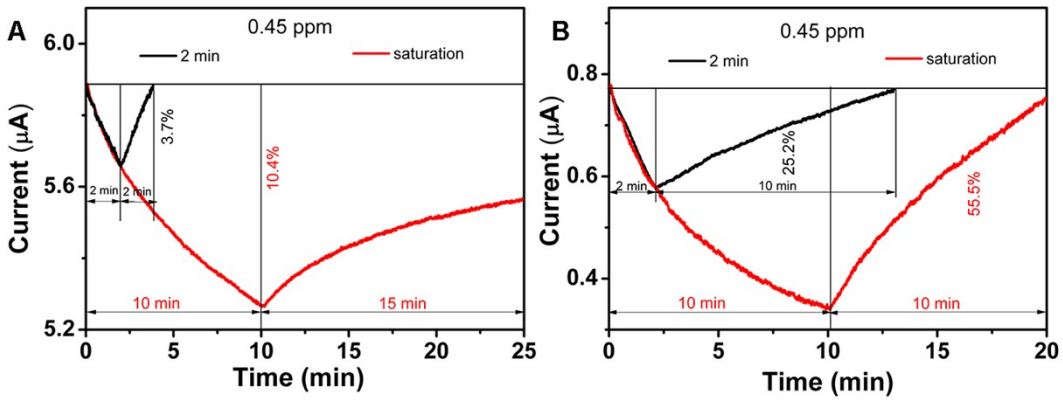

Fig.S9. The response of the devices for compound **1**(A)-**2**(B) under 0.45 ppm NO_2 exposure of 2 min and 10 min.

Table S1. The orientation angle of the phthalocyanine ring determined from polarized UV-vis absorbance of the LS films of compounds **1-2**.

Compound	A//	A⊥	D 0° (A///A⊥)	A//	A⊥	D 45° (A// A⊥)	θ°
1	0.156	0.162	0.96	0.150	0.179	0.84	64.7
2	0.145	0.127	1.14	0.106	0.131	0.81	28.1

Table S2. The gate-induced sheet carrier densities (n) of the LS films of compounds **1-2**.

Cpds	n_e/cm^{-2} (0 V)[a]	n_h/cm^{-2} (0 V)[a]	n_e/cm^{-2} (40 V)[a]	n_h/cm^{-2} (40 V)[a]
1	2.48×10^{12}	8.31×10^{9}	7.68×10^{13}	1.03×10^{12}
2	1.77×10^{12}	8.01×10^{10}	4.52×10^{12}	3.90×10^{12}

[a] Calculated from $n = (I_{ds}/V_{ds})(L/W)(1/\mu e)$, where I_{ds} is the source–drain current, V_{ds} the source–drain voltage, W the channel width(28.6 mm), L the channel length (0.24 mm), μ the carrier mobility.

In the present system, the carrier densities were calculated at V_G=0 V and 40 V, respectively. The values of (I_{ds}/V_{ds}) is the slope values of linear region of output characterics when V_G=0 V and 40 V, respectively. As seen in Table S2, both n_e and n_h at 40 V are higher than n_e and n_h at 0 V, which means the gate voltage is an important influence factor of carrier densities. However, no matter 0 V or 40 V,

the n_e of **2** is always smaller than n_e of **1**, the n_h of **1** is always smaller than n_h of **2**. Note that in the main text, only the carrier densities at V_G=0 V were listed in Table 2, representing an original status before gases inject.